Atmos. Chem. Phys. Discuss., 14, 27195–27231, 2014
www.atmos-chem-phys-discuss.net/14/27195/2014/
doi:10.5194/acpd-14-27195-2014


Atmospheric Chemistry and Physics Discussions



# Radiative forcing and climate metrics for ozone precursor emissions: the impact of multi-model averaging

**C. R. MacIntosh, K. P. Shine, and W. J. Collins**

Department of Meteorology, University of Reading, P.O. Box 243, Reading, RG6 6BB, UK

Received: 19 September 2014 – Accepted: 10 October 2014 – Published: 29 October 2014

Correspondence to: C. R. MacIntosh (c.r.macintosh@reading.ac.uk)

Published by Copernicus Publications on behalf of the European Geosciences Union.







## Abstract

Multi-model ensembles are frequently used to assess understanding of the response of ozone and methane lifetime to changes in emissions of ozone precursors such as $NO_x$, VOC and CO. When these ozone changes are used to calculate radiative forcing (RF) (and climate metrics such as the global warming potential (GWP) and global temperature potential (GTP)) there is a methodological choice, determined partly by the available computing resources, as to whether the mean ozone (and methane lifetime) changes are input to the radiation code, or whether each model's ozone and methane changes are used as input, with the average RF computed from the individual model RFs. We use data from the Task Force on Hemispheric Transport of Air Pollution Source-Receptor global chemical transport model ensemble to assess the impact of this choice for emission changes in 4 regions (East Asia, Europe, North America and South Asia).

We conclude that using the multi-model mean ozone and methane responses is accurate for calculating the mean RF, with differences up to 0.6 % for CO, 0.7 % for VOC and 2 % for $NO_x$. Differences of up to 60 % for $NO_x$ 7 % for VOC and 3 % for CO are introduced into the 20 year GWP as a result of the exponential decay terms, with similar values for the 20 years GTP.

However, estimates of the SD calculated from the ensemble-mean input fields (where the SD at each point on the model grid is added to or subtracted from the mean field) are almost always substantially larger in RF, GWP and GTP metrics than the true SD, and can be larger than the model range for short-lived ozone RF, and for the 20 and 100 year GWP and 100 year GTP. We find that the effect is generally most marked for the case of $NO_x$ emissions, where the net effect is a smaller residual of terms of opposing signs. For example, the SD for the 20 year GWP is two to three times larger using the ensemble-mean fields than using the individual models to calculate the RF.






ACPD
14, 27195–27231, 2014



Hence, while the average of multi-model fields are appropriate for calculating mean RF, GWP and GTP, they are not a reliable method for calculating the uncertainty in these fields, and in general overestimate the uncertainty.

## 1 Introduction

Ozone is an important radiatively active gas. Changes in tropospheric ozone since pre-industrial times contribute between 0.2 and 0.6 $W m^{-2}$ to present day radiative forcing (RF) (Stevenson et al., 2013). Ozone is a secondary product of photochemical reactions resulting from emissions of precursor species, such as CO, volatile organic compounds (VOCs), $NO_x$, and methane. These ozone precursor species themselves have large associated measurement, source and sink uncertainties (e.g. Cuesta et al., 2013; Kirschke et al., 2013), and widely differing atmospheric lifetimes (from days to a decade). The resulting ozone perturbation can therefore have highly spatially inhomogeneous distributions, both in the horizontal and vertical, with the result that confidence in the spatial pattern of ozone RF is only described as medium in the Intergovernmental Panel on Climate Change (IPCC) Fifth Assessment Report (Myhre et al., 2013).

Climate metrics provide an important method of comparing the mean climate effects of emissions of various forcing agents. The Global Warming Potential (GWP) is defined by IPCC as the time-integrated radiative forcing due to a 1 kg pulse emission at time horizon $H$ relative to an equivalent emission of $CO_2$ (Myhre et al., 2013). The Global Temperature-change Potential (GTP) describes the surface temperature change at time horizon $H$ in a similar fashion (Shine et al., 2005). Both of these metrics depend strongly on the chosen time horizon.

Metrics for ozone precursors remain challenging to compute, due to the spatial inhomogeneity of the forcing, the large uncertainties associated with the perturbation of ozone and methane concentrations, and the fact that the metric depends on where and when the species is emitted. In the particular case of $NO_x$, the RF due to short-term ozone change and the longer term methane and primary-mode ozone changes are of





ACPD
14, 27195–27231, 2014



opposite signs; therefore the RF, GWP and GTP are smaller residuals of two larger terms (e.g. Fuglestvedt et al., 2010).

The dependence on the location of the emissions change (e.g. Collins et al., 2013) has its origins in the spatially-varying background chemistry, and in variations in insolation and temperature which also contribute to non-linearities in chemical behaviour. Model intercomparison studies which perturb, either individually or together, a number of ozone precursor species can provide a useful constraint on our understanding of the effect of changing emissions of SLCF species on tropospheric ozone. The Hemispheric Transport of Air Pollutants (HTAP) project perturbed individual ozone precursor species in different regions with a view to elucidating transport of short lived pollutants (Task Force on Hemispheric Transport of Air Pollution, 2010). Subsequent work by Fry et al. (2012) and Collins et al. (2013) assessed the RF, GWP and GTP for the precursor species. Computational limitations prevented the analysis of the variability in the RF, GWP and GTP using output from individual models in Fry et al. (2012); instead the ensemble-mean $\pm\sigma$ fields of the ozone perturbation were used as a representative subset of the complete ensemble.

In the present work, we calculate the RF, GWP and GTP using output from each individual model in the HTAP ensemble. We then compare our results to those obtained with the model ensemble-mean ozone and methane $\pm\sigma$ fields using the method of Fry et al. (2012). This approach assesses the extent to which the RF calculated with the mean ozone fields represents the mean of the RF calculated using the ozone fields from each model individually; it also elucidates whether the uncertainty in RF computed using the $\pm\sigma$ ozone fields correctly represents the uncertainty that emerges from the calculations using each model individually.

Section 2 introduces the data used in this study, and describes the set up of the radiation code, Sect. 3 presents the initial precursor, ozone and methane fields, Sect. 4 discusses radiative forcing, Sect. 5 presents the metrics, and conclusions are given in Sect. 6.





ACPD
14, 27195–27231, 2014



## 2 Methods

An ensemble of model runs from the HTAP study provides information on ozone and methane concentrations after a perturbation in an ozone precursor gas has been applied. Initial results and analysis are presented in Fiore et al. (2009). Here the resulting tropospheric ozone (together with calculated methane and ozone primary mode, PM) changes are used to calculate RF for each model and scenario using the Edwards–Slingo radiation code (Edwards and Slingo, 1996). The model ensemble mean and SD fields are calculated both before and after the RF calculations, for the individual ozone, methane and ozone PM fields.

As this study is concerned with understanding methodological uncertainty we do not account for the effects of the precursor emissions on stratospheric ozone or water vapour. In addition, the contribution of sulphate aerosol changes, as a result of the precursor emissions, which were included in the HTAP calculations, are not included here.

### 2.1 Models

The HTAP study perturbation scenarios reduced by 20 % emissions of short-lived ozone precursor gases $NO_x$, CO and VOC in four different regions (North America, Europe, South Asia and East Asia), and a further run in which methane concentrations were perturbed globally. There are therefore 13 scenarios. Table 1 shows the HTAP nomenclature for the experiments, and the locations of the source regions. 11 chemistry transport models (CTMs) (see Table 2) produced results for these scenarios. For comparison with previous literature, the 11 models used in our study are the same as those used in Fry et al. (2012) and Collins et al. (2013) (Table 2).

Of the 11 CTMs used in this study, 9 use meteorological background fields from reanalyses to drive the model, while two (STOC-HadAM3-v01 and UM-CAM-v01) are coupled to global climate models (GCMs) and use 2001 sea ice and sea surface temperature data to drive the GCM. The models also use a variety of sources for the base-





ACPD
14, 27195–27231, 2014



line emissions data, with the result that a 20 % decrease in emissions is not equivalent in mass terms between models. This serves to characterise the uncertainty due to emissions and model differences simultaneously; however, separation of the two effects is not possible here.

The model output is re-gridded to a common resolution of 2.75° latitude × 3.75° longitude, with 24 vertical levels, which is comparable to the resolution of the models on average. Many of the models do not fully resolve the stratosphere; therefore stratospheric changes in all species are neglected, and, above the tropopause, the models share a common climatology.

## 2.2 Radiation code

Model output is at monthly-mean resolution for the year 2001. For each model, January, April, July and October are used as input to the code, in order to reduce run-time constraints whilst remaining sufficient to resolve the annual cycle in transport and RF. Sensitivity tests have shown that the ozone PM and methane RFs are almost completely insensitive to increasing the number of months included (less than 1 part in 1000), and the short-lived ozone RFs have a sensitivity of the order of 0.5 % to increasing the number of months. Table S4 provides a brief outline of the sensitivity tests.

The Edwards–Slingo radiation code uses the two stream approximation to calculate radiative transfer through the atmosphere. Clouds are included in the code. Nine broadband channels in the longwave and 6 channels in the shortwave are used. Incoming solar radiation at mid-month, and Gaussian integration over 6 intervals is used to simulate variation in the diurnal cycle.

A common background climatology supplying temperature and humidity are taken from the European Centre for Medium-Range Weather Forecasts reanalyses (Dee et al., 2011). Mean cloud properties from the International Satellite Cloud Climatology Project (ISCCP) are also used for all RF simulations (Rossow and Schiffer, 1999).





ACPD
14, 27195–27231, 2014



RF is calculated as the difference in the net flux at the tropopause (defined as the level at which the lapse rate falls below 2 K km$^{-1}$), after the stratospheric temperature has been allowed to adjust using the standard fixed dynamical heating method (e.g. Fels et al., 1980).

The mean RF and associated uncertainty calculated using the individual model ozone and methane perturbation fields is denoted by $\overline{\mathrm{RF}}$. The RF calculated using the ensemble-mean ozone and methane perturbations, and the associated uncertainty, as was done by Fry et al. (2012), is denoted by $\mathrm{RF}_{(\mathrm{EN}\pm\sigma)}$. In the present calculations the RF due to the individual short-lived ozone, PM ozone and methane are calculated, for each model and the total is the sum of these components. Sensitivity tests have shown that the total RF is very close (within 0.5 %) to the sum of the individual contributions from the component gases.

This approach differs from Fry et al. (2012), where the RF due to the total (ensemble-mean) ozone and methane changes is computed using their radiation code. The individual components are then computed via a "back-calculation". The methane RF for each scenario is calculated from the change in methane concentration using the simple formula of Ramaswamy et al. (2001); the difference between the total RF and this methane RF is then attributed to ozone, although the methane RF using the radiation code may differ somewhat from that deduced using the simple formula. For the calculation of metrics, it is further necessary to separate the ozone RF between the short-lived and PM components, which Fry et al. (2012) achieve by using the ("back-calculated") ozone forcing calculated using the SR2 results, scaled by the ratio of the (global-mean) ozone change between a given scenario and the SR2 scenario. For consistency with Fry et al. (2012) the individual components of the $\mathrm{RF}_{(\mathrm{EN}\pm\sigma)}$ are computed in the same way here.

### 2.3 Climate metrics

The methodology for calculation of the climate metrics (GWPs and GTPs) follows that described in Fuglestvedt et al. (2010), including the same impulse-response func-





ACPD
14, 27195–27231, 2014



tion for carbon dioxide, and the climate impulse-response function sensitivities from Boucher and Reddy (2008) which is needed for the GTP calculation. The effect of the uncertainties in these impulse response functions are not explored here. The metric calculations require the steady-state RF per unit emission per year, for each pre-cursor and for the short-lived ozone, PM ozone and methane changes individually. Again the technique for deriving these from the steady-state perturbations follows Fuglestvedt et al. (2010). The resulting steady-state RFs for each model and each scenario are given in the Supplement. The nomenclature for the metrics follows that for the RF described in the previous subsection.

## 3 Ozone and methane input fields

The CTMs produce [OH], [$O_3$] and associated atmospheric loss rates as 3-D output fields. Short-lived ozone can be used directly as input to the radiation code. Methane fields for each model and each simulation were globally homogeneous, and fixed at 1760 ppbv, except in the $CH_4$ scenario, when they are reduced to 1408 ppbv. Equilibrium methane concentrations for each scenario can be calculated from the change in methane lifetime, $\Delta\alpha$, as $[CH_4] = 1760 \times (\frac{\alpha_{\text{control}}+\Delta\alpha}{\alpha_{\text{control}}})^f$, where the methane lifetimes are calculated from the $CH_4$ x OH fluxes (since the atmospheric OH sink accounts for around 90 % of loss of atmospheric $CH_4$, and surface sinks are considered constant). The feedback factor, $f$ is determined in Fiore et al. (2009) from the change in loss rates between the control and the $CH_4$ perturbation scenarios, and accounts for the effect of methane change on its own lifetime (Prather, 1996).

Ozone PM changes are dependent on the change in ozone resulting from a change in methane, which in turn depends on the change in methane lifetime for a given scenario. The PM changes for each model and scenario are calculated as described in West et al. (2009) by scaling the ozone change in the $CH_4$ perturbation simulation by the relative change in methane concentration as given in Fiore et al. (2009).





ACPD
14, 27195–27231, 2014



Table 2 shows the control-run methane lifetimes, the feedback factor and the change in methane lifetime between the control and the $CH_4$ perturbation experiment for each model and the ensemble mean. The methane lifetime varies by about 20 %, from around 8 to 10 years, with the exception of the LLNL-IMPACT-T5a model, which has a much shorter lifetime of around 5.5 years. The feedback factor has a variability of around 10 %, with no substantial outliers. The multi-model mean $\pm\sigma$ ozone, methane and ozone PM fields are constructed by calculating the SD for each grid box and adding/subtracting this from the ensemble mean to generate the 3-D SD fields. In contrast to the individual model runs above, where each gas is run separately through the radiation code, RF due to the combined effect of the total ozone and the methane field is calculated. The RF due to the individual species is then back-calculated as described in Sect. 2.2.

To test whether the model ensemble mean $\pm\sigma$ input fields can be used to generate climate metrics that are representative of the model ensemble, we must first establish the extent to which the ensemble mean $\pm\sigma$ represents the input fields. Figure 1 shows the short-lived ozone annual-average mass changes for the 10 or 11 individual models used in this study (note that INCA VOC, SA region, and LLNL $NO_x$, all regions, are missing in the input fields).

The multi-model mean and SD short-lived ozone mass change, and the true mean and SD are shown in red and blue respectively. The mean values are identical in both cases, as expected. The two sets of error bars denote the model SD calculated in two different ways. Those in blue show the SD calculated from the global-average burden change for each individual model. Those in red show the area-average of the 3-D grid-point-level SD fields. The global average of the grid-point level SD fields is not equal to the SD calculated after the global mean for each model has been calculated, i.e. the order of operations in this case makes a substantial difference to the $\pm 1\sigma$ error bars. For any set of fields, the true SD will always be overestimated by the area-average of the 3-D SD. The relative size of the difference will depend on the inhomogeneity in the 3-D fields.





ACPD
14, 27195–27231, 2014



The ozone mass change fields are spatially inhomogeneous in both the horizontal and the vertical. Of the three precursor species, $NO_x$ is the most short-lived, and has the highest degree of spatial inhomogeneity. Therefore the difference between the two methods of SD calculations is largest in the ozone fields for the $NO_x$ case. For a completely homogeneous field (in $kg\,m^{-3}$), there would be no difference in SD between the two methods. The largest SDs relative to the mean are found for the VOC case, in part due to large differences between the models in terms of VOC speciation and chemistry schemes (e.g. Collins et al., 2002).

It should also be noted that the spatial distribution of the ozone fields $\pm 1\sigma$ error bars is not necessarily representative of any single, individual model. Figure 2 shows the deviation from the ensemble-mean column integrated ozone field for the $NO_x$ NA case. The top three rows show the deviation from the ensemble mean for each ensemble member, and the bottom row shows the same for the ensemble mean and SD fields. By construction, the deviation from the mean is everywhere positive for the positive case, and always negative for the negative cases. However, for any individual model, there can be both positive and negative deviations and for only a few models do their deviations resemble the ensemble-mean case. Therefore the resulting RF fields from the ensemble-mean calculation may not be expected to provide a realistic representation of the spread of forcings about the mean, when individual model ozone fields are used to calculate the forcing.

## 4 Radiative forcing

Figure 3 shows the RF for all 11 models, for the short-lived ozone, primary-mode ozone and methane for each scenario. In the case of $NO_x$, the total RF is a small residual as the ozone and methane forcings act in opposite directions. The $\overline{RF}$ for $NO_x$ varies from $1.62\,mW\,m^{-2}$ for NA to $-1.02\,mW\,m^{-2}$ for EA and SA (Table 3). RF due to ozone, methane and ozone PM for any individual model is largest in NA, and smallest in EU or SA, consistently across the model ensemble. This larger sensitivity of global-mean RF





ACPD
14, 27195–27231, 2014



(relative to the VOC and CO cases) to emission location is due to the short lifetime of $NO_x$ relative to VOC and CO. Note that the total RF for $NO_x$ may not reflect the size of the RF response of the components. For example the EA region has the second largest ozone, methane and PM RF, but the smallest (with SA) total RF response (Fig. 4).

For VOC and CO, the methane and ozone RF act in the same direction. The global-mean RF is less dependent on the location of the emission for the CO case than for the $NO_x$ or VOC cases. The variation in $\overline{RF}$ between $-3.99\,mW\,m^{-2}$ for EA and $-2.24\,mW\,m^{-2}$ for EU is almost entirely due to variations in the emission mass in each region, with the RF per unit mass emission change being about $0.14\,mW\,m^{-2}(Tg(CO)\,year^{-1})^{-1}$ for all four regions (Table S2). CO has an atmospheric lifetime of around 3 months, which is of the same order as the hemispheric atmospheric mixing time. The SD for any given emission region is smaller relative to the mean than in the $NO_x$ and VOC cases being around 30 % of the mean for all four regions, and all of the models are in the same ranking order in each of the four regions. As the distribution of CO is relatively homogeneous, differences in the model RFs come largely from the initial mass change in the ozone precursor species and the efficiency of its removal from the atmosphere.

Confidence in the chemistry of each species can be inferred from the variability across the model ensemble. VOC has a very large range of short-lived ozone estimates. In the EA and EU regions, for example, the SD of the short-lived ozone change is around 0.25 Tg, for an ensemble-mean mass change of around 0.35 Tg (see Fig. 1). This large variability is in large part due to different chemistry and speciation schemes across the model ensemble, in addition to the wide range of estimates of VOC mass emission changes (e.g. Frost et al., 2013).

The forcing for the $CH_4$ perturbation scenario (bottom panel of Fig. 3) comprises only the methane and ozone PM contributions, since there is no short-lived ozone forcing from a change in methane. The methane RF is identical ($-0.14\,W\,m^{-2}$) across all models, as they have the same mixing-ratio change, but differ in the ozone PM RF, which depends on the chemistry schemes of the models. The global ozone mass





ACPD
14, 27195–27231, 2014



change varies almost by a factor of 2, from 7.5 Tg for the MOZARTGFDL-v2 model to 16 Tg for LLNL-IMPACT-T5a, with associated RF of 25.4 and 54.9 mW $m^{-2}$ respectively.

The RF due to methane for a given scenario depends on the methane lifetime in the model, and the change in methane lifetime for the particular scenario. The VOC scenarios have the largest relative uncertainty in the methane changes ($\sigma$ = 59 to 104 % of the mean), including one model (GISS-PUCCINI-modelE) which has a small increase in methane due to a decrease in VOC in three of the regions (NA, EA and EU, Fig. 3).

The ozone PM RF depends on the scaling of the ozone PM mass change from the $CH_4$ perturbation scenario by the relative change in methane for each scenario, and therefore is also related to $\Delta\alpha$ in addition to the model ozone response to a change in methane; hence it has a slightly larger relative uncertainty than the methane changes due to model differences in ozone PM response.

Short-lived ozone has the largest variability of the three components across the ensemble for any scenario, and the largest normalised variability for $NO_x$ and CO. For VOC, short-lived ozone is the largest single contributor to the total RF, whereas for $NO_x$ and CO, methane dominates. The SD in ozone response is between ±24 % in EA to ±42 % (SA) of the mean for $NO_x$, ±58 % (SA) to ±77 % (NA) for VOC and ±27 % (SA) to ±37 % (NA) for CO (Table S1). A large relative short-lived ozone response to one precursor species is not a good indicator of the response to other perturbations. For a particular species, however, models with a large response in one region will tend to have a large response in all regions, i.e the models all agree on the order of the regional responses. These depend on the relative size of emissions change in each region and the mass-normalised RF. This is a good indicator of consistency across different emissions datasets and for transport in models, which information cannot be gained by using the model ensemble mean alone.

For $NO_x$, there is a positive correlation between the size of the methane response and the short-lived ozone response, with $r^2$ values between 0.56 (EA) to 0.86 (SA) (Table S1). For VOC and CO, the coefficients are much smaller (0.01 (NA) to 0.52 (SA) for VOC, and close to zero for all CO cases except EU). For $NO_x$, there is significant





ACPD
14, 27195–27231, 2014



correlation between the short-lived ozone and methane responses, even if the emission mass for each model is taken into account, with $r^2$ values between 0.70 (EA) and 0.86 (NA and SA, Table S2). This suggests that the individual model chemistry may dominate over variability in emissions data.

### 4.1 Ensemble-mean RF measures

Table 3 compares $\overline{\mathrm{RF}} \pm \sigma$ with the computationally much less intensive $\mathrm{RF}_{(\mathrm{EN}\pm\sigma)}$. Differences between the means are only of the order of a few percent, with the largest differences found for the $NO_x$ EA case of 3 %. For VOC and CO, the differences between the means does not exceed 0.7 %, and for $CH_4$, the difference is negligible. The larger fractional difference in the case of $NO_x$ is due to the fact that the means are a small residual of two much larger components. Hence $\mathrm{RF}_{(\mathrm{EN}\pm\sigma)}$ is representative of the true ensemble mean, $\overline{\mathrm{RF}}$. By contrast the SD in the $\overline{\mathrm{RF}} \pm \sigma$ case is smaller for every scenario relative to $\mathrm{RF}_{(\mathrm{EN}\pm\sigma)}$. This is largely associated with the inability of the pre-calculated ensemble mean fields to represent the true model spread, as described in Sect. 3.

Figure 4 separates the total RF into components due to the ozone PM, methane, and short-lived ozone contributions, for each scenario and gas, for the $\mathrm{RF}_{(\mathrm{EN}\pm\sigma)}$ and $\overline{\mathrm{RF}} \pm \sigma$.

In the $CH_4$ perturbation case, the absolute methane RFs (red bars) have no uncertainty associated with intermodel differences because the methane concentration change is fixed. The RF calculated using the formula of Ramaswamy et al. (2001) is $-139.6\,\mathrm{mW\,m^{-2}}$ for $\mathrm{RF}_{(\mathrm{EN})}$, whereas the value calculated by the Edwards–Slingo radiation code for $\overline{\mathrm{RF}}$ is slightly more negative at $-141\,\mathrm{mW\,m^{-2}}$. Because of the "back-calculation" method described in Sect. 2.2 this results in the estimate of the ozone PM $\mathrm{RF}_{(\mathrm{EN})}$ being 5 % too negative ($-37.0\,\mathrm{mW\,m^{-2}}$ vs. $-35.3\,\mathrm{mW\,m^{-2}}$). The SD of the $CH_4$ scenario ozone PM $\mathrm{RF}_{(\mathrm{EN})}$ is 33 % of the mean, compared with 24 % for the $\overline{\mathrm{RF}}$ case. As the $CH_4$ scenario ozone PM RF is used to calculate the PM RF for each scenario for





ACPD
14, 27195–27231, 2014



the EN case, and the PM RF is used to calculate the short-lived ozone RF, this small error will propagate through all the EN RF estimates. The effect is very small however, with the overestimate in short-lived ozone RF being between 1.6 and 2.4 % (NA and EU) in the $NO_x$ scenarios, between −0.02 and 1.1 % (NA, EU) for VOC, and 1.7 and 2.9 % (NA, SA respectively) for CO.

The relative sizes of the SDs for the methane, ozone PM and short-lived ozone RFs are mostly governed by the increased spread in the input fields as described in Sect. 3. For the methane RF in the $NO_x$, VOC and CO scenarios, the SD $RF_{(EN\pm\sigma)}$ is slightly smaller than the $\overline{RF}$ SD in all regions, although the difference is less than 1.5 %. This is due to the smaller methane contribution in the $RF_{(EN)}$ case, resulting in a smaller absolute SD. If the SD is normalised relative to the mean for each scenario, then the $RF_{(EN)}$ SD is essentially identical to the $\overline{RF}$ SD.

The ozone PM SD is about 30 % larger for the $RF_{(EN)}$ case relative to the $\overline{RF}$ case, reflecting its relatively greater spatial inhomogeneity as discussed in Sect. 3. The $RF_{(EN)}$ SD is between 35–42 % of the mean (depending on the source region) for $NO_x$, 33–106 % for VOC and 37–57 % for the CO scenarios. For $\overline{RF}$ the values are 26–32 % for $NO_x$, 62–96 % for VOC and 26–44 % for CO.

The short-lived ozone RF $\pm\sigma$ shows the greatest difference between the two methods, again reflecting the difference in the input fields in Sect. 3. The largest absolute reductions, in SD occur for the $NO_x$ cases, since these are the most spatially inhomogeneous fields; the SD is 45–58 % and 24–42 % (EA, SA) of the mean for $RF_{(EN)}$ and $\overline{RF}$ respectively.

The relatively greater uncertainty surrounding the size of the VOC scenario response is reflected in the larger SDs, from 76–94 % and 58–77 % in the $RF_{EN}$ and $\overline{RF}$ cases. Finally for the CO cases, the SDs vary between 51–56 % and 27–37 % in the two cases. The difference in the short-lived ozone SDs is the major driving factor of the differences in the total $RF_{(EN)}$ and $\overline{RF}$ SDs in Table 3.





ACPD
14, 27195–27231, 2014



## 5 Climate metrics

### 5.1 Global warming potentials

GWPs are calculated as described in Sect. 2. The uncertainty estimates for the back-calculated and ensemble-mean GWPs are calculated as described for the GWPs in Collins et al. (2013), and account explicitly for uncertainty in the RF response and in the total methane lifetime ($\tau$) variability, where $\tau = \alpha f$. These are denoted $\mathrm{GWP}_{(\mathrm{EN}\pm\sigma)}$, while the the true values are denoted $\overline{\mathrm{GWP}} \pm \sigma$.

Table 4 gives the 20 year $\overline{\mathrm{GWP}} \pm \sigma$ and $\mathrm{GWP}_{(\mathrm{EN}\pm\sigma)}$ for each scenario. $\mathrm{NO_x}$ 20 year $\overline{\mathrm{GWP}}$ varies from −27 in SA to −3 in EA, and the sign is not robust in NA, SA or EA for either $\overline{\mathrm{GWP}}$ or $\mathrm{GWP}_{(\mathrm{EN})}$. The large variability is attributable to the competing effects of the long- and short-lived components. The VOC 20 year mean GWP estimates fall between 16 to 22 and for CO between 5.0 and 5.8.

The magnitude of the 20 year $\overline{\mathrm{GWP}}$ can be either larger or smaller than the $\mathrm{GWP}_{(\mathrm{EN})}$. For $\mathrm{NO_x}$ and CO, $\mathrm{GWP}_{(\mathrm{EN})}$ is larger by 4.1 (EU) to 57.6 % (EA) and 0.7 (EU) to 3.4 % (SA) respectively, and smaller for $\mathrm{CH_4}$ and VOC by 0.9 % and 4.1 (EA) to 7.3 % (SA) respectively.

Figure 5 shows the relative contributions of each component to the total 20 year GWP. For $\mathrm{NO_x}$, the methane plus ozone PM GWP is larger than the short-lived ozone GWP, resulting in negative net GWP. For the $\mathrm{GWP}_{(\mathrm{EN})}$ the short-lived GWP is smaller relative to the long-lived GWP (from 67 (EU) to 96 % (EA), relative to 69 (EU) to 98 % (SA) for $\overline{\mathrm{GWP}}$), giving a more negative net GWP. For VOC, short-lived ozone dominates, being between 121 (EU) to 239 % (EA) and 125 (EU) to 240 % (EA) of the long-lived GWP for the $\mathrm{GWP}_{(\mathrm{EN})}$ and $\overline{\mathrm{GWP}}$ respectively. Finally for CO, the long-lived GWP dominates, with the short-lived ozone being 47 (EU) to 73 % (SA) and 48 (EU) to 70 % (SA) of the long-lived GWP for the two estimates

The $\mathrm{GWP}_{(\mathrm{EN})}$ SD accounts for uncertainty due to $\mathrm{CH_4}$, $\mathrm{O_3}$ PM and short-lived ozone, and changes in methane lifetime. For all regions and scenarios, the $\mathrm{GWP}_{(\mathrm{EN})}$ SD is





ACPD
14, 27195–27231, 2014



larger than that for the $\overline{\text{GWP}}$ (Table 4, Fig. 5, top row). Figure 5 also shows the SD for each scenario that is due to ozone PM, methane and short-lived ozone (second, third and bottom row, respectively). The $\text{GWP}_{(\text{EN})}$ SD is larger than that for $\overline{\text{GWP}}$, for most components. The larger SD in the short-lived ozone $\text{RF}_{(\text{EN})}$ relative to $\overline{\text{RF}}$ is also apparent in the GWP values, and once again is the major driver of the larger uncertainty in the overall $\text{GWP}_{(\text{EN})}$.

Uncertainty in methane lifetime is only a minor contributor to the overall uncertainty in $\text{GWP}_{(\text{EN})}$. For example, in the $\text{NO}_x$ NA case, the SD due to the short-lived ozone is ±44, due to methane RF is ±20, due to ozone PM is ±9 and due to methane lifetime effects is ±5, with similar behaviour for other regions and species. There is an anti-correlation across the model ensemble between $\alpha$ and $f$ of −0.72, which is significant at the 95 % level. This means that the total methane lifetime, $\tau$ is smaller than it would be were these quantities to be truly independent, as is therefore the variability attributed to $\tau$.

Table 5 gives the 100 year GWP. The magnitude of $\text{GWP}_{(\text{EN})}$ is again larger for the $\text{NO}_x$ and CO cases, and smaller for the $\text{CH}_4$ and VOC cases (except SA), but the difference is much reduced relative to the 20 year GWP, not exceeding 8 % (VOC NA) of the total GWP.

In the case of the 100 year $\text{GWP}_{(\text{EN})}$, the long-term component is a simple scaling of the 20 year GWP by the ratio of the exponential terms and by $\frac{100\,\text{year AGWP CO}_2}{20\,\text{year AGWP CO}_2}$. The normalised $\frac{\sigma}{\text{GWP}}$ is therefore identical at 20 and 100 year for the $\text{CH}_4$, ozone PM and short-lived ozone components, (and is also identical to the $\frac{\sigma}{\text{RF}_{\text{EN}}}$). The total normalised SD for the $\text{GWP}_{(\text{EN})}$ case is slightly smaller (26–35 % for CO, 59–70 % for VOC and 54–135 % for $\text{NO}_x$, relative to 28–36 %, 63–71 % and 93–992 % for the equivalent 20 year GWP values, regions as for 20 years). In contrast, for $\overline{\text{GWP}}$, the normalised SD is increased by 2 to 5 % in the 100 year GWP relative to the 20 year GWP for the VOC





ACPD
14, 27195–27231, 2014



and CO scenarios, as differences in the methane lifetime have a larger impact, although there is a substantial reduction in the $NO_x$ SD (Table S3).

For short-lived ozone, for both $\overline{GWP}$ and $GWP_{(EN)}$ the scaling factor is simply $\frac{100\,\text{year AGWP CO}_2}{20\,\text{year AGWP CO}_2}$, and the normalised SDs are again identical to those for the 20 year GWP. The relative contribution of the short-lived ozone to the GWP is therefore slightly smaller at 100 years than at 20 years, being 38–59 % for CO, 97–146 % for VOC and 54–76 % for $NO_x$, relative to 47–73 %, 121–181 % and 67–96 % (all EU, SA) at 20 years. The consistency in the regional response across the scenarios and metrics suggests that the latitude of the emissions affects the relative importance of the short- and long-lived components.

For the 100 year $\overline{GWP}$ components (not shown), the normalised uncertainty for the short-lived ozone is identical to that at 20 years, but the $CH_4$ and ozone PM $\frac{\sigma}{\overline{GWP}}$ is slightly larger, due to the increased importance of the methane lifetime.

The smaller uncertainty associated with the total $\overline{GWP}$ $NO_x$ results in the values at 100 years being robustly negative, in contrast with the $GWP_{(EN)}$ case. This is primarily due to the reduced uncertainty for the short-lived ozone contribution, and the poor representation of uncertainty in RF in the ensemble-mean case.

### 5.2 Global temperature-change potentials

The 20 year GTP mean values (Table 6) share many characteristics with the GWP values, including the reduction in uncertainty of $\overline{GTP}$ relative to $GTP_{(EN\pm\sigma)}$ in most cases.

Figure 6 shows the total, short-lived ozone, methane and ozone PM components for the 20 year $GTP_{(EN)}$ and $\overline{GTP}$. One important difference relative to the 20 year GWP is that the $NO_x$ GTP is robustly negative in all cases, due to the much larger contribution of the methane component.





ACPD
14, 27195–27231, 2014



The long-lived components of the 100 year GTP (Table 7) are related to the 20 years GTP in the same way that the 100 and 20 year GWPs are related. The long-lived component is a much larger fraction of the 20 year GTP than it is of the 100 year GTP, since 20 years is close to the methane response time (~ 12 years). This arises since the GTP is not a time integrated quantity, and the relative contribution of the components to the overall temperature change depends also on the climate response at its timescales.

### 5.3 Comparison of GWP and GTP time evolution for $NO_x$

Figure 7 shows the time evolution of the GWP (top) and GTP (bottom) for the $NO_x$ SA region. Coloured lines show the evolution of each model, with the solid black line and dotted lines giving the true mean and SD. The dashed lines and grey shading give the $GWP_{(EN\pm\sigma)}$.

Models which have a longer methane lifetime have a steeper GWP gradient at 20 years than models with a short methane lifetime; however, this is not necessarily a good indicator of a more negative $NO_x$ GWP at 20 years. Of the four longest lifetime models, three (CAMCHEM-3311m13, UM-CAM-v01 and MOZECH-v16) have GWP values that are more positive than the mean, with the fourth (GISS-PUCCINI-modelE) lying well within one SD. This indicates that they also have a large short-lived ozone forcing.

GWP has its largest SD between 10 and 30 years, when both short-lived ozone and methane forcings are important. The $GWP_{(EN)}$ overestimates the true SD everywhere, but particularly around 10–30 years. At these timescales, the SDs produced in this way lie outside the range of the ensemble members, and therefore are not a good estimate of the uncertainty of the ensemble.

The GTP (lower panel in Fig. 7) does not have the same "memory" of early forcing as the GWP, so that the model spread decreases substantially after about 30 years. The separate effects of a long methane lifetime and a large short-lived ozone forcing can be more clearly seen here for UM-CAM-v01 (yellow line), which has a very neg-





ACPD
14, 27195–27231, 2014



ative minimum GTP value of less than −200, several years after the other ensemble members.

The largest uncertainty in the GTP is also around 20 years, when both the short-lived ozone, methane and ozone PM RF are important. Again, the $GTP_{(EN)}$ substantially overestimates the uncertainty betwen 10 and 30 years. At times greater than about 35 years, however, the $GTP_{(EN)}$ begins to agree better with the true $\overline{GTP}$. The $GTP_{(EN)}$ may even slightly underestimate the uncertainty at these longer times due to the slightly smaller methane RF estimate calculated in Sect. 4.

## 6 Discussion and conclusions

This study has investigated the derivation of RF and climate emission metrics (GWP and GTP at various time horizons) for emissions of short-lived climate forcing agents from multi-model assessments, using the results of the HTAP ozone precursor emission experiments as an example. Multi-model means and their associated SDs of the ozone perturbations can be used as input to radiative transfer codes, which is clearly more computationally efficient than calculating the radiative forcing for each model individually and averaging the results. Overall, our results indicate that the order of averaging does not have a major impact on the mean values. It does, however, have a larger impact on estimates of the uncertainties.

The global-mean RF from emissions of ozone precursors is only mildly sensitive to using the ensemble-mean input fields with differences in the mean not exceeding 3 %. However, the SD of the RF is rather distinct between the two cases. The true SD (using the RF derived from each model individually) is always smaller than the SD when calculating the RF with the ensemble-mean ozone change. This effect is mostly due to the construction of the input ozone fields overestimating the true ensemble spread. In the case of the ozone PM, the $RF_{(EN)}$ SD is about 30 % larger than the true value. For the more spatially inhomogeneous short-lived ozone, the overestimate varies between 20 % for the VOC EA scenario to 90 % for the $NO_x$ EA case.





ACPD
14, 27195–27231, 2014



The $GWP_{(EN)}$ and $GTP_{(EN)}$ mean values agree well with the true mean as might be expected from the RF estimates, the difference not exceeding 10 % for VOC and CO, although they can be somewhat larger (up to 60 % in EA) for $NO_x$. This approach may therefore be sufficient for some purposes given the computational saving that may be achieved, particularly with larger ensembles.

For estimates of uncertainty, however, there is substantial disagreement between the two methods. The overestimate of uncertainty associated with the short- and long-lived ozone RF propagates to the climate metrics. These terms are the dominant cause of the increased uncertainty, rather than methane lifetime effects. For all time horizons, the uncertainty in $GWP_{(EN)}$ is not only substantially larger than the $\overline{GWP}$, but lies outside of the range covered by the model ensemble itself. Therefore this approach should not be used when deriving the uncertainty in GWP.

There is a similar overestimate of the uncertainty in the GTP at short time horizons due to the short-lived ozone and ozone PM; however, at time horizons greater than about 40 years, the ozone forcing becomes relatively less important to the GTP, and the uncertainty in $GTP_{(EN)}$ is more in line with the true uncertainty estimate.

**The Supplement related to this article is available online at doi:10.5194/acpd-14-27195-2014-supplement.**

*Acknowledgements.* We acknowledge funding from the European Commission, under the ECLIPSE (Evaluating the Climate and Air Quality Impacts of Short-Lived Pollutants) Project (Grant Agreement 282688) and thank other ECLIPSE partners for their input to this work. We acknowledge the contribution of those involved in the HTAP CTM simulations, performed under the UN ECE Task Force on Hemispheric Transport of Air Pollution.





ACPD
14, 27195–27231, 2014



## References


Boucher, O. and Reddy, M.: Climate trade-off between black carbon and carbon dioxide emissions, Energ. Policy, 36, 193–200, doi:10.1016/j.enpol.2007.08.039, 2008. 27202

Collins, W., Derwent, R., Johnson, C., and Stevenson, D.: The oxidation of organic compounds in the troposphere and their global warming potentials, Climatic Change, 3, 453–479, doi:10.1023/A:1014221225434, 2002. 27204

Collins, W. J., Fry, M. M., Yu, H., Fuglestvedt, J. S., Shindell, D. T., and West, J. J.: Global and regional temperature-change potentials for near-term climate forcers, Atmos. Chem. Phys., 13, 2471–2485, doi:10.5194/acp-13-2471-2013, 2013. 27198, 27199, 27209

Cuesta, J., Eremenko, M., Liu, X., Dufour, G., Cai, Z., Höpfner, M., von Clarmann, T., Sellitto, P., Foret, G., Gaubert, B., Beekmann, M., Orphal, J., Chance, K., Spurr, R., and Flaud, J.-M.: Satellite observation of lowermost tropospheric ozone by multispectral synergism of IASI thermal infrared and GOME-2 ultraviolet measurements over Europe, Atmos. Chem. Phys., 13, 9675–9693, doi:10.5194/acp-13-9675-2013, 2013. 27197

Dee, D., Uppala, S., Simmons, A., Berrisford, P., Poli, P., Kobayashi, S., Andrae, U., Balmaseda, M., Balsamo, G., Bauer, P., Bechtold, P., Beljaars, A., van de Berg, L., Bidlot, J., Bormann, N., Delsol, C., Dragani, R., Fuentes, M., Geer, A., Haimberger, L., Healy, S., Hersbach, H., Holm, E., Isaksen, L., Kalbers, P., Kohler, M., Matricardi, M., McNally, A., Monge-Sanz, B., Morcrette, J.-J., Park, B.-K., Peubey, C., de Rosnay, P., Tavolato, C., Thepaut, J.-N., and Vitart, F.: The ERA-Interim reanalysis: configuration and performance of the data assimilation system, Q. J. Roy. Meteor. Soc., 137, 553–597, doi:10.1002/qj.828, 2011. 27200

Edwards, J. and Slingo, A.: Studies with a flexible new radiation code. 1: Choosing a configuration for a large-scale model, Q. J. Roy. Meteor. Soc., 122, 689–719, doi:10.1002/qj.49712253107, 1996. 27199

Fels, S. B., J. D. Mahlman, J., M. D. Schwarzkopf, M., and Sinclair, R.: Stratospheric sensitivity to perturbations in ozone and carbon dioxide: radiative and dynamical response, J. Atmos. Sci., 37, 2265–2297, doi:10.1175/1520-0469(1980)037<2265:SSTPIO>2.0.CO;2, 1980. 27201

Fiore, A. M. and West, J., Horowitz, L., Naik, V., and Schwarzkopf, M.: Multimodel estimates of intercontinental source-receptor relationships for ozone pollution, J. Geophys. Res., 113, D04301, doi:10.1029/2008JD010816, 2009. 27199, 27202, 27219






ACPD
14, 27195–27231, 2014



Frost, G., Middleton, P., Tarrason, L., Granier, C., Guenther, A., Cardenas, B., van der Gon, H., Janssens-Maenhout, G., Kaiser, J., Keating, T., Klimont, Z., Lamarque, J.-F., Liousse, C., Nickovic, S., Ohara, T., Schultz, M., Skiba, U., van Aardenne, J., and Wang, Y.: New Directions: GEIA's 2020 vision for better air emissions information, Atmos. Environ., 81, 710–712, doi:10.1016/j.atmosenv.2013.08.063, 2013. 27205

Fry, M. M., Naik, V., Schwarzkopf, J. J. W. M. D., Fiore, A. M., Collins, W. J., Dentener, F. J., Shindell, D. T., Atherton, C., Bergmann, D., Duncan, B. N., Hess, P., MacKenzie, I. A., Marmer, E., Schultz, M. G., Szopa, S., Wild, O., and Zeng, G.: The influence of ozone precursor emissions from four world regions on tropospheric composition and radiative climate forcing, J. Geophys. Res., 117, D07306, doi:10.1029/2011JD017134, 2012. 27198, 27199, 27201, 27221, 27228, 27229, 27231

Fuglestvedt, J. S., Shine, K. P., Berntsen, T., Cook, J., Lee, D., Stenke, A., Skeie, R., Velders, G., and Waitz, I.: Transport impacts on atmosphere and climate: Metrics, Atmos. Environ., 44, 4648–4677, doi:10.1016/j.atmosenv.2009.04.044 2010. 27198, 27201, 27202

Kirschke, S., Bousquet, P., Ciais, P., Saunois, M., Canadell, J. G., Dlugokencky, E. J., Bergamaschi, P., Bergmann, D., Blake, D. R., Bruhwiler, L., Cameron-Smith, P., Castaldi, S., Chevallier, F., Feng, L., Fraser, A., Heimann, M., Hodson, E. L., Houweling, S., Josse, B., Fraser, P. J., Krummel, P. B., Lamarque, J.-F., Langenfelds, R. L., Quere, C. L., Naik, V., O'Doherty, S., Palmer, P. I., Pison, I., Plummer, D., Poulter, B., Prinn, R. G., Rigby, M., Ringeval, B., Santini, M., Schmidt, M., Shindell, D. T., Simpson, I. J., Spahni, R., Steele, L. P., Strode, S. A., Sudo, K., Szopa, S., van der Werf, G. R., Voulgarakis, A., van Weele, M., Weiss, R. F., Williams, J. E., and Zeng, G.: Three decades of global methane sources and sinks, Nat. Geosci., 6, 813–823, doi:10.1038/NGEO1955, 2013. 27197

Myhre, G., Shindell, D., Breon, W., Collins, W., Fuglestvedt, J., Huang, J., Koch, D., Lamarque, J.-F., Lee, B. M., Nakajima, T., Robock, G., Stephens, G., Takemura, T., and Zhang, H.: Anthropogenic and natural radiative forcing, in: Climate Change 2013: The Physical Science Basis. Contribution of Working Group I to the Fifth Assessment Report of the Intergovernmental Panel on Climate Change, Cambridge University Press, 8, 659–740, 2013. 27197

Prather, M.: Time scales in atmospheric chemistry: theory, GWPs for $CH_4$ and CO, and runaway growth, Geophys. Res. Lett., 23, 2597–2600, doi:10.1029/96GL02371, 1996. 27202

Ramaswamy, V., Boucher, O., Haigh, J., Hauglustaine, D., Haywood, J., Myhre, G., Nakajima, T., Shi, G., and Solomon, S.: Radiative forcing of climate change, in: Climate Change 2001: The Scientific Basis. contribution of Working Group 1 to the Third Assessment Report of the





ACPD
14, 27195–27231, 2014



Intergovernmental Panel on Climate Change, edited by: Houghton, J., Ding, Y., Griggs, D., Noguer, M., van der Linden, P., Dai, X., Maskell, K., and Johnson, C., 349–416, Cambridge university Press, Cambridge, U. K., 2001. 27201, 27207

Rossow, W. and Schiffer, R.: Advances in understanding clouds from ISCCP, B. Am. Meteorol. Soc., 80, 2261–2288, doi:10.1175/1520-0477(1999)080<2261:AIUCFI>2.0.CO;2, 1999. 27200

Shine, K., Fuglestvedt, J. S., Hailemariam, K., and Stuber, N.: Altermatives to the Global Warming Potential for comparing climate impacts of emissions of greenhouse gases, Clim. Change, 68, 281–302, doi:10.1007/s10584-005-1146-9 2005. 27197

Stevenson, D. S., Young, P. J., Naik, V., Lamarque, J.-F., Shindell, D. T., Voulgarakis, A., Skeie, R. B., Dalsoren, S. B., Myhre, G., Berntsen, T. K., Folberth, G. A., Rumbold, S. T., Collins, W. J., MacKenzie, I. A., Doherty, R. M., Zeng, G., van Noije, T. P. C., Strunk, A., Bergmann, D., Cameron-Smith, P., Plummer, D. A., Strode, S. A., Horowitz, L., Lee, Y. H., Szopa, S., Sudo, K., Nagashima, T., Josse, B., Cionni, I., Righi, M., Eyring, V., Conley, A., Bowman, K. W., Wild, O., and Archibald, A.: Tropospheric ozone changes, radiative forcing and attribution to emissions in the Atmospheric Chemistry and Climate Model Intercomparison Project (ACCMIP), Atmos. Chem. Phys., 13, 3063–3085, doi:10.5194/acp-13-3063-2013, 2013. 27197

Task Force on Hemispheric Transport of Air Pollution: Hemispheric Transport of Air Pollution, U.N. Econ. Comm. for Europe, Geneva, Switzerland, 2010. 27198

West, J. J., Naik, V., Horowitz, L. W., and Fiore, A. M.: Effect of regional precursor emission controls on long-range ozone transport – Part 2: Steady-state changes in ozone air quality and impacts on human mortality, Atmos. Chem. Phys., 9, 6095–6107, doi:10.5194/acp-9-6095-2009, 2009. 27202





ACPD
14, 27195–27231, 2014



**Table 1.** HTAP ozone precursor anthropogenic reduction experiments. In the case of SR2, methane mixing ratios are reduced by 20 %; for SR3-SR5 emissions of the precursor are reduced. The regions are defined as: North America (NA), 15–55° N, 60–125° W; South Asia (SA), 5–35° N, 50–95° E East Asia (EA), 15–50° N, 95–160° E; Europe (EU), 25–65° N, 10° W–50° E.

| Experiment | Region | Description |
|---|---|---|
| SR1 | Global | Control |
| SR2 | Global | −20 % $CH_4$ reduction |
| SR3 | NA, SA, EA, EU | −20 % $NO_x$ reduction |
| SR4 | NA, SA, EA, EU | −20 % VOC reduction |
| SR5 | NA, SA, EA, EU | −20 % CO reduction |





ACPD
14, 27195–27231, 2014



**Table 2.** Methane lifetime ($\alpha$), feedback factor ($f$), and the methane lifetime change due to a 20 % global reduction in methane, for each of the 11 CTMs, and the ensemble mean and SD, as calculated in Fiore et al. (2009). Model abbreviations are explained in Fiore et al. (2009).

| Model | Methane Lifetime $\alpha$ (years) | Feedback Factor $f$ | Lifetime Change $\Delta\alpha_{SR2}$ (years) |
|---|---|---|---|
| CAMCHEM-3311m13 | 10.11 | 1.31 | 0.51 |
| FRSGCUCI-v01 | 7.72 | 1.43 | 0.50 |
| GISS-PUCCINI-modelE | 9.39 | 1.36 | 0.54 |
| GMI-v02f | 9.02 | 1.31 | 0.46 |
| INCA-vSSz | 8.75 | 1.31 | 0.45 |
| LLNL-IMPACT-T5a | 5.68 | 1.39 | 0.34 |
| MOZARTGFDL-v2 | 9.06 | 1.31 | 0.47 |
| MOZECH-v16 | 9.63 | 1.29 | 0.48 |
| STOC-HadAM3-v01 | 8.20 | 1.31 | 0.42 |
| TM5-JRC-cy2-ipcc-v1 | 7.98 | 1.43 | 0.51 |
| UM-CAM-v01 | 10.57 | 1.25 | 0.45 |
| Mean | 8.73 | 1.33 | 0.47 |
| SD | ±1.34 | ±0.06 | ±0.05 |





ACPD
14, 27195–27231, 2014



**Table 3.** Total RF$\pm\sigma$ (mW m$^{-2}$) for each scenario. The SD values given for $RF_{(EN)}$ are the RF resulting from the mean and standard deviation ozone, methane and ozone PM fields, as described in Sect. 3. The true SD values for $\overline{RF}$ are calculated after the total RF for each model in each scenario has been calculated; therefore they are not equal to the sum of the SD for each component gas.

| Scenario | type | NA mean | $\sigma$ | SA mean | $\sigma$ | EA mean | $\sigma$ | EU mean | $\sigma$ |
|---|---|---|---|---|---|---|---|---|---|
| $NO_x$ (SR3) | $\overline{RF}$ | 1.62 | ±2.43 | 1.02 | ±1.76 | 1.02 | ±1.58 | 1.50 | ±1.12 |
| | $RF_{(EN)}$ | 1.65 | ±3.03 | 1.05 | ±2.13 | 1.05 | ±2.27 | 1.52 | ±1.52 |
| VOC (SR4) | $\overline{RF}$ | −1.50 | ±1.28 | −1.16 | ±0.68 | −1.49 | ±1.11 | −1.82 | ±1.50 |
| | $RF_{(EN)}$ | −1.50 | ±1.41 | −1.15 | ±0.80 | −1.48 | ±1.25 | −1.82 | ±1.69 |
| CO (SR5) | $\overline{RF}$ | −3.03 | ±1.22 | −2.52 | ±0.61 | −3.99 | ±1.61 | −2.24 | ±0.68 |
| | $RF_{(EN)}$ | −3.04 | ±1.46 | −2.53 | ±0.87 | −4.00 | ±1.98 | −2.24 | ±0.88 |
| | | Global | | | | | | | |
| $CH_4$ (SR2) | $\overline{RF}$ | −176.6 | ±8.4 | | | | | | |
| | $RF_{(EN)}$ | −176.5 | ±12.1 | | | | | | |





ACPD
14, 27195–27231, 2014



**Table 4.** Ensemble-mean 20 year GWP. The true mean GWP and SD are denoted $\overline{\text{GWP}} \pm \sigma$. The GWP calculated using the method described in Fry et al. (2012) is denoted $\text{GWP}_{(\text{EN}\pm\sigma)}$. Average methane lifetimes used in the metric construction are given in Table 2.

| Scenario | type | NA mean | $\sigma$ | SA mean | $\sigma$ | EA mean | $\sigma$ | EU mean | $\sigma$ |
|---|---|---|---|---|---|---|---|---|---|
| $NO_x$ (SR3) | $\overline{\text{GWP}}$ | −9.76 | ±15.5 | −27.4 | ±34.1 | −2.64 | ±20.7 | −20.6 | ±7.85 |
| | $\text{GWP}_{(\text{EN})}$ | −11.4 | ±41.2 | −30.1 | ±98.0 | −4.15 | ±41.2 | −21.5 | ±20.1 |
| VOC (SR4) | $\overline{\text{GWP}}$ | 17.6 | ±8.10 | 21.2 | ±8.20 | 16.9 | ±7.99 | 17.2 | ±7.42 |
| | $\text{GWP}_{(\text{EN})}$ | 16.3 | ±11.7 | 22.1 | ±13.9 | 16.2 | ±10.5 | 16.0 | ±10.6 |
| CO (SR5) | $\overline{\text{GWP}}$ | 5.22 | ±1.20 | 5.59 | ±0.98 | 5.27 | ±1.09 | 4.99 | ±1.24 |
| | $\text{GWP}_{(\text{EN})}$ | 5.32 | ±1.86 | 5.78 | ±1.63 | 5.30 | ±1.94 | 5.03 | ±1.47 |
| | | Global | | | | | | | |
| $CH_4$ (SR2) | $\overline{\text{GWP}}$ | 64.9 | ±4.17 | | | | | | |
| | $\text{GWP}_{(\text{EN})}$ | 64.3 | ±5.18 | | | | | | |





ACPD
14, 27195–27231, 2014



**Table 5.** As Table 4 for the 100 year GWP.

| Scenario | type | NA mean | $\sigma$ | SA mean | $\sigma$ | EA mean | $\sigma$ | EU mean | $\sigma$ |
|---|---|---|---|---|---|---|---|---|---|
| $NO_x$ (SR3) | $\overline{GWP}$ | −10.8 | ±4.77 | −23.1 | ±9.83 | −8.62 | ±6.58 | −10.7 | ±2.67 |
| | $GWP_{(EN)}$ | −11.2 | ±12.0 | −23.7 | ±28.9 | −8.75 | ±11.8 | −10.9 | ±5.86 |
| VOC (SR4) | $\overline{GWP}$ | 5.45 | ±2.54 | 6.62 | ±2.57 | 5.17 | ±2.54 | 5.40 | ±2.41 |
| | $GWP_{(EN)}$ | 5.04 | ±3.52 | 6.86 | ±4.06 | 4.94 | ±3.14 | 5.05 | ±3.33 |
| CO (SR5) | $\overline{GWP}$ | 1.72 | ±0.42 | 1.82 | ±0.34 | 1.73 | ±0.38 | 1.66 | ±0.45 |
| | $GWP_{(EN)}$ | 1.74 | ±0.59 | 1.87 | ±0.49 | 1.76 | ±0.62 | 1.66 | ±0.47 |
| | | Global | | | | | | | |
| $CH_4$ (SR2) | $\overline{GWP}$ | 23.0 | ±2.41 | | | | | | |
| | $GWP_{(EN)}$ | 22.7 | ±1.56 | | | | | | |





ACPD
14, 27195–27231, 2014



**Table 6.** As Table 4 for the 20 years GTP.

| Scenario | type | NA mean | σ | SA mean | σ | EA mean | σ | EU mean | σ |
|---|---|---|---|---|---|---|---|---|---|
| $NO_x$ (SR3) | $\overline{GTP}$ | −62.8 | ±16.6 | −122.1 | ±36.3 | −59.3 | ±19.0 | −42.8 | ±8.38 |
| | $GTP_{(EN)}$ | −62.9 | ±19.1 | −122.3 | ±46.8 | −57.8 | ±17.1 | −42.8 | ±9.5 |
| VOC (SR4) | $\overline{GTP}$ | 8.98 | ±4.61 | 11.19 | ±4.31 | 7.99 | ±4.49 | 9.44 | ±4.68 |
| | $GTP_{(EN)}$ | 8.25 | ±5.57 | 11.54 | ±5.62 | 7.66 | ±4.80 | 8.93 | ±6.24 |
| CO (SR5) | $\overline{GTP}$ | 3.39 | ±0.92 | 3.52 | ±0.70 | 3.43 | ±0.80 | 3.39 | ±0.97 |
| | $GTP_{(EN)}$ | 3.49 | ±1.16 | 3.62 | ±0.79 | 3.50 | ±1.21 | 3.42 | ±0.90 |
| | | Global | | | | | | | |
| $CH_4$ (SR2) | $\overline{GTP}$ | 55.3 | ±5.49 | | | | | | |
| | $GTP_{(EN)}$ | 54.8 | ±3.77 | | | | | | |





ACPD
14, 27195–27231, 2014



**Table 7.** As Table 4 for the 100 year GTP.

| Scenario | type | NA mean | σ | SA mean | σ | EA mean | σ | EU mean | σ |
|---|---|---|---|---|---|---|---|---|---|
| $NO_x$ (SR3) | $\overline{GTP}$ | −2.20 | ±0.79 | −4.53 | ±1.64 | −1.87 | ±1.04 | −1.92 | ±0.44 |
| | $GTP_{(EN)}$ | −2.22 | ±1.75 | −4.55 | ±4.23 | −1.84 | ±1.71 | −1.93 | ±0.86 |
| VOC (SR4) | $\overline{GTP}$ | 0.81 | ±0.38 | 0.98 | ±0.38 | 0.76 | ±0.38 | 0.81 | ±0.37 |
| | $GTP_{(EN)}$ | 0.74 | ±0.51 | 1.01 | ±0.58 | 0.72 | ±0.46 | 0.75 | ±0.50 |
| CO (SR5) | $\overline{GTP}$ | 0.26 | ±0.07 | 0.28 | ±0.05 | 0.26 | ±0.06 | 0.25 | ±0.07 |
| | $GTP_{(EN)}$ | 0.26 | ±0.09 | 0.28 | ±0.07 | 0.27 | ±0.09 | 0.25 | ±0.07 |
| | | Global | | | | | | | |
| $CH_4$ (SR2) | $\overline{GTP}$ | 3.62 | ±0.45 | | | | | | |
| | $GTP_{(EN)}$ | 3.55 | ±0.27 | | | | | | |





ACPD
14, 27195–27231, 2014



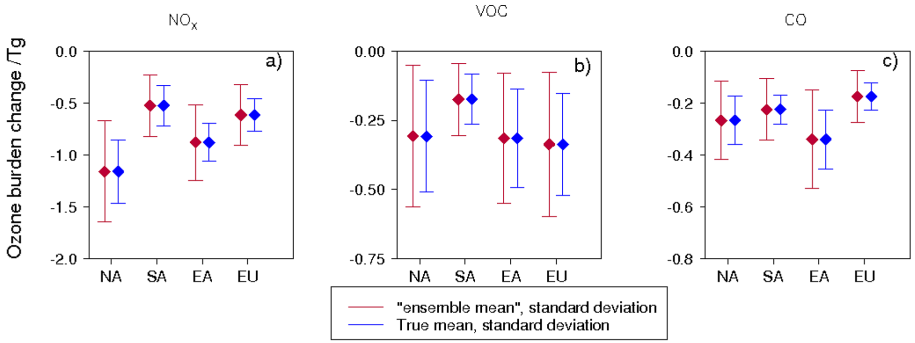


**Figure 1.** Change in global-mean atmospheric burden of short-lived ozone (in Tg), for **(a)** $NO_x$, **(b)** VOC, and **(c)** CO for the emission changes and emission regions given in Table 1. The "ensemble mean" and SD fields (red lines) are constructed by calculating the mean and SD of the model ensemble at each grid point.





ACPD
14, 27195–27231, 2014



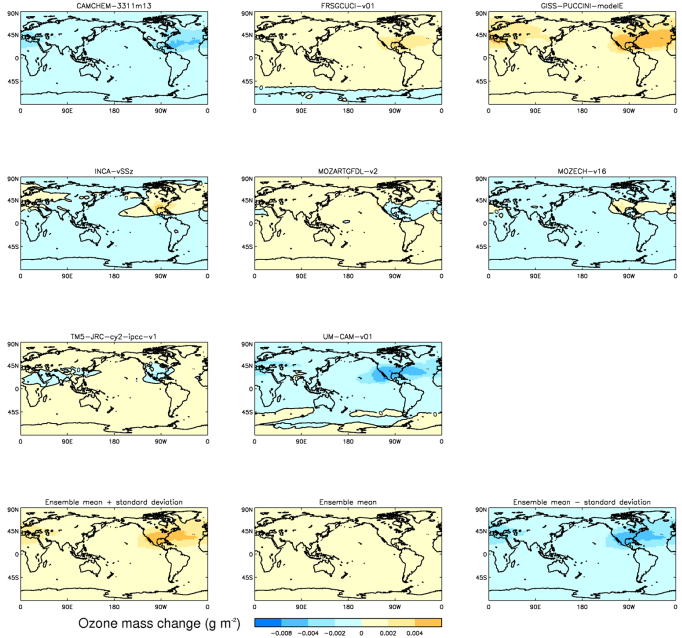


**Figure 2.** Spatial distribution of the deviation from the ensemble mean in annual-mean column integrated short-lived ozone perturbation ($g\,m^{-2}$) for the $NO_x$ NA case (see Table 1) for each individual model (top three rows). The bottom row shows the ensemble mean deviation (centre, by definition this is zero everywhere) and the plus (left) and minus (right) one SD from this mean.





ACPD
14, 27195–27231, 2014

Radiative forcing and climate metrics for ozone precursor emissions

C. R. MacIntosh et al.



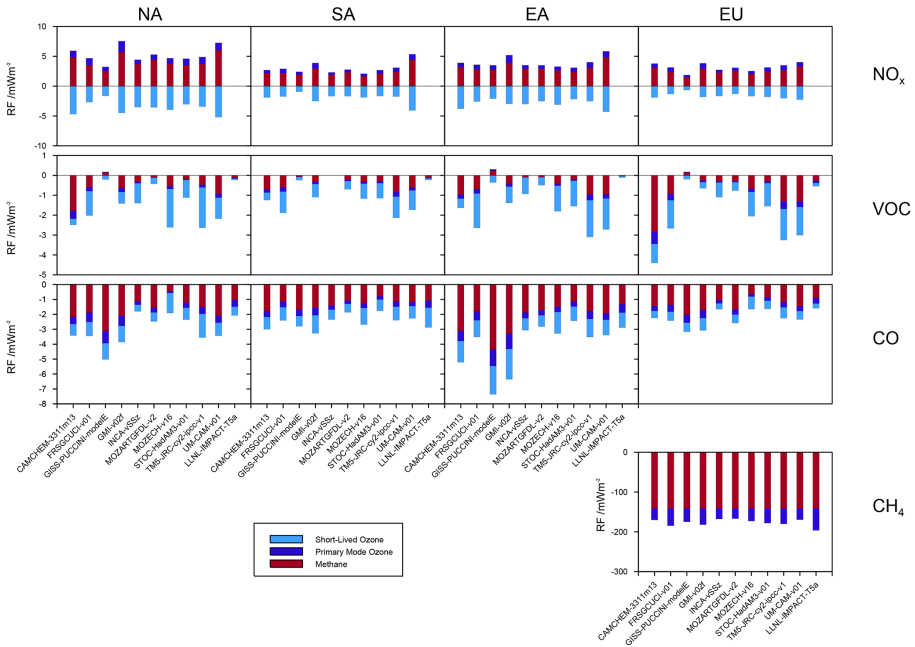


**Figure 3.** Radiative forcing for $NO_x$ (first row), VOC (second row), CO (third row), and $CH_4$ (bottom), for each of the 11 models, for each of the four regions given in Table 1. Methane forcings (bottom row) are given as if resulting from a perturbation of methane emissions – see text for details. Units are mW m$^{-2}$. Colours show RF due to short-lived ozone (light blue), methane (red) and primary mode ozone (dark blue).





ACPD
14, 27195–27231, 2014



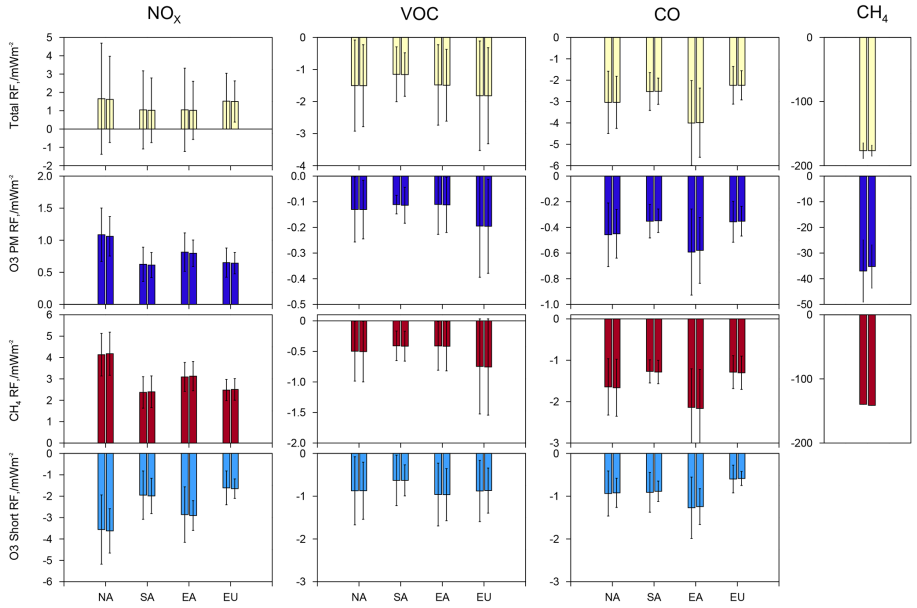


**Figure 4.** Ensemble-mean radiative forcing for (first column) $NO_x$, (second column) VOC, (third column) CO, and (right) $CH_4$, for (top, yellow) total RF, (second row, dark blue) RF due to ozone PM, (third row, red) RF due to methane, and (bottom row, pale blue) RF due to short-lived ozone. For each pair of bars, the right-hand bar denotes the true mean, $\overline{RF}$, and the left-hand bar gives the ensemble value calculated using the method of Fry et al. (2012), $RF_{(EN)}$. Units are $mW\,m^{-2}$.





ACPD
14, 27195–27231, 2014



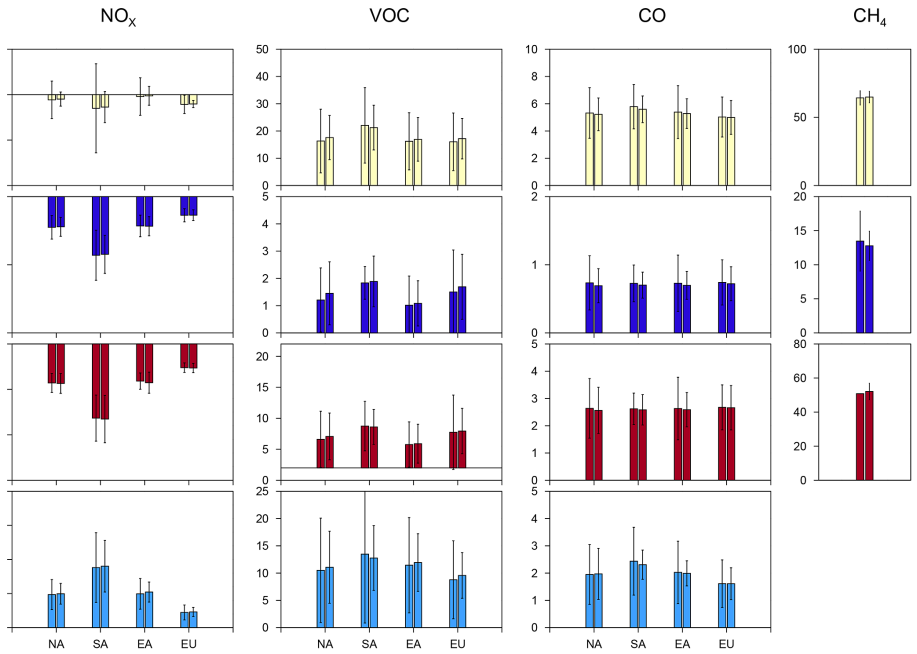


**Figure 5.** 20 year GWP for (first column) $NO_x$, (second column) VOC, (third column) CO, and (right) $CH_4$, for (top, yellow) total GWP, (second row, dark blue) GWP due to ozone PM, (third row, red) GWP due to methane, and (bottom row, pale blue) GWP due to short-lived ozone. For each pair of bars, the right-hand bar denotes the true mean, $\overline{GWP}$, and the left-hand bar gives the ensemble value calculated using the method of Fry et al. (2012), $GWP_{(EN)}$.





ACPD
14, 27195–27231, 2014



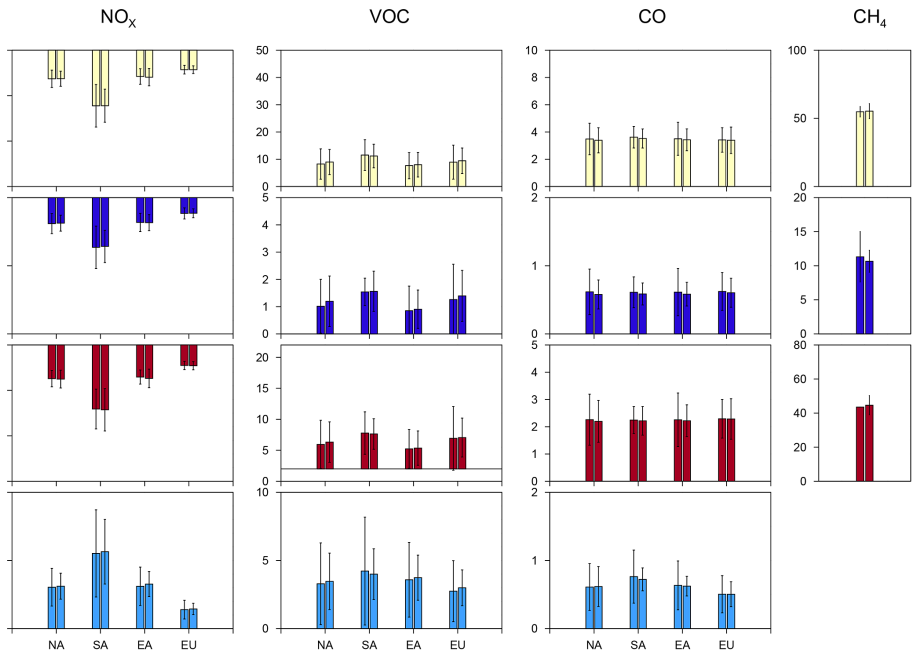


**Figure 6.** 20 years GTP for (first column) $NO_x$, (second column) VOC, (third column) CO, and (right) $CH_4$, for (top, yellow) total GTP, (second row, dark blue) GTP due to ozone PM, (third row, red) GTP due to methane, and (bottom row, pale blue) GTP due to short-lived ozone. For each pair of bars, the right-hand bar shows $\overline{GTP}$, and the left-hand bar shows, $GTP_{(EN)}$.





ACPD
14, 27195–27231, 2014



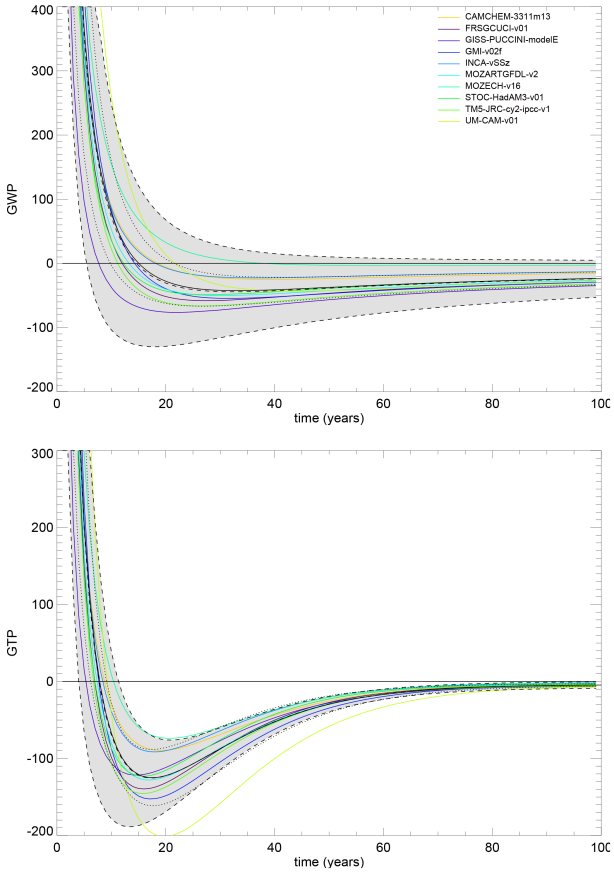


**Figure 7.** Time evolution of (top) GWP and (bottom) GTP for the $NO_x$ SA case, showing each model. The solid black line and surrounding dotted lines represent the model ensemble mean and SD. The dashed lines and shaded area represent the mean and SD using the method of Fry et al. (2012).





ACPD
14, 27195–27231, 2014